Research Article

Jérôme Bourderionnet*, Arnaud Brignon, Daniel Dolfi and Jean-Pierre Huignard

Mid-infrared laser beam steering based on Fourier transform OPO

DOI 10.1515/aot-2016-0064
Received December 2, 2016; accepted February 13, 2017; previously published online March 15, 2017

Abstract: Inertia-less optical scanners are an essential building block for many systems, including remote sensing, spectroscopy, and optronics. Although many solutions provide efficient scanning devices in the visible to near-infrared spectral range today, none of these devices offers good performances in longer wavelengths like in the mid-IR range. The new rationale that is described in this paper is to take advantage of existing and well-proven steering techniques in the near IR and to reach mid-IR by frequency conversion in a specifically designed Fourier transform optical parametric oscillator.

Keywords: beam steering; mid-infrared; parametric oscillators and amplifiers.

1 Introduction

Fast and accurate steering of laser beams enable applications like laser-based sensing, communications, and power projection. Traditional opto-mechanical scanners suffer from the inertia issue, which limits their speed, and increase the cost and size of the systems. Worldwide research and development activities, therefore, focus on the realization of nonmechanical compact beam steering devices with large optical apertures, low weight, low power, high agility, multi-spectral capability, and large field of regard [1].

***Corresponding author: Jérôme Bourderionnet,** Thales Research and Technology, 1 Avenue A. Fresnel, 91767 Palaiseau, France, e-mail: jerome.bourderionnet@thalesgroup.com
Arnaud Brignon and Daniel Dolfi: Thales Research and Technology, 1 Avenue A. Fresnel, 91767 Palaiseau, France
Jean-Pierre Huignard: Jphopto, 20 rue Campo Formio, 75013 Paris, France

Many solutions have been proposed and demonstrated. For instance, acousto-optic cells provide efficient deflectors, where the laser beam diffracts under Bragg condition on an acoustically induced index grating [2, 3]. Electro-optic (EO) prism architectures have also been reported, exploiting Pockels or Kerr effect in an EO material. The limited EO index change, however, limits the number of resolved scanning directions to a few tens [4–6]. Recently, devices exploiting liquid crystal (LC) huge birefringence, however, showed impressive performances [7]. Finally, phased array architectures have also raised a large interest for beam-steering purpose, either based on LC cells [8], or EO material, like PLZT or PMN-PT [9, 10].

The reported and commercial nonmechanical scanners offer today efficient ways to steer a laser beam in the visible to near-infrared spectral range, but there is a broad range of applications, like remote sensing, spectroscopy, imaging, and countermeasures, which require beam scanning in the 3 μm to 5 μm range. Unfortunately, none of these existing solutions operate in this spectral band. LC, indeed, suffers from the C-H bond absorption peak in liquid crystal molecules, while AO cell diffraction efficiency drops dramatically as the wavelength increases. PLZT and PMN-PT are transparent in the 3- to 5-μm range and could offer a possibility, but with a substantial increase in driving voltage in phased array implementation.

To overcome these issues, we propose in this paper to perform the beam-steering functionality in a spectral window where commercial device efficiency is well established (at 1 μm in the present work), and frequency converts this scanned beam to the 3- to 5-μm range using an optical parametric oscillator (OPO) [11, 12] in a specific Fourier transform (FT) configuration. After introducing the FT-OPO concept and its design guidelines, we report the experimental demonstration of mid-IR nonmechanical beam scanning. The system performances are evaluated both in terms of scanning functionality (resolved directions, 2D and multitarget steering capability) and frequency conversion (OPO efficiency and beam quality).

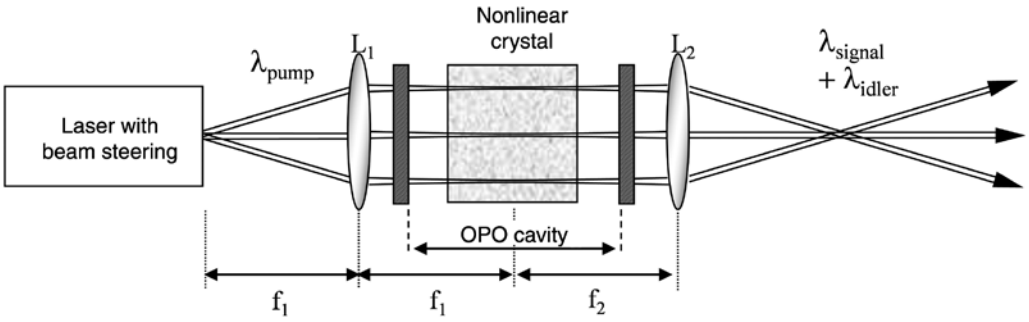

Figure 1: Schematic of the Fourier transform optical arametric oscillator (FT-OPO).

2 Fourier transform optical parametric oscillator

2.1 Principle

The principle of this concept is to convert a deflected beam at 1 μm wavelength into a deflected beam at a longer wavelength by means of a specially designed OPO. The advantage of this scheme is that the beam-steering device is used at 1 μm, where several efficient beam-steering techniques are already available, such as acousto-optic (AO) beam deflector. The OPO then converts the steered beam in the mid-infrared wavelength of interest (such as 1.5 μm or 3- to 5-μm spectral range).

Wavelength conversion is realized with OPOs in nonlinear crystals that possess a very low acceptance angle. The so-called FT-OPO [13] is specially designed to deal with this issue and convert the deflected pump beam, as described in Figure 1.

The basic idea is to convert a deflection into a displacement. This operation is performed by a Fourier operation that can be obtained in the two focal planes of a lens. The nonlinear crystal is placed in the focal planes of two lenses L1 and L2. The deflected pump beam at 1 μm, therefore, enters the nonlinear crystal at a constant angle of incidence whatever the beam direction is, for optimized wavelength conversion. The second lens L2 allows deflecting the converted beam. The two lenses should have proper focal lengths to control the beam divergence of the deflected beams.

In the following section, the design guidelines of the FT-OPO are derived. In particular, the trade-off between the number of resolved points and the maximum pump energy that can be launched into the OPO crystal is discussed, depending on its laser-induced damage (LID) threshold.

2.2 FT-OPO design and analysis

2.2.1 Number of resolved directions and maximum pump energy

In this work, the FT-OPO is pumped by a laser operating at 1.06 μm and delivers a signal beam around 1.5 μm and an idler around 3.5 μm. The most important parameters for the system are the number of resolved points in the scanning field and the maximum pump energy that can be launched into the OPO without LID. The number of resolved points per dimension (horizontal or vertical) is defined by the ratio of the maximum scanning angle and the scanned beam divergence and is expressed here by:

$$N = \frac{D}{2\omega_0} \times \sqrt{\frac{2}{\ln 2}}$$

where D is the nonlinear crystal full size in one direction, and ω_0 is the beam radius at $1/e^2$ of the pump beam at 1.06 μm. On another hand, the maximum pump energy to avoid LID is given by:

$$E_{\max} = \mathrm{LIDT} \times \pi\omega_0^2$$

where LIDT is the LID threshold of the OPO. Equations (1) and (2) finally give the relation between the number of resolved directions and the maximum pump energy:

$$N = D \times \sqrt{\frac{\pi \times \mathrm{LIDT}}{2\ln 2 \times E_{\max}}}$$

The dependence of N with $E_{\max}$ is plotted in Figure 2, for a nonlinear crystal aperture of 1.5×1.5 cm^2 and for LIDT values ranging from 1 to 10 J/cm^2.

In particular, considering an OPO crystal having an aperture size $D = 1.5$ cm and a typical value of 5 J/cm^2 for the LIDT, we can conclude the following:

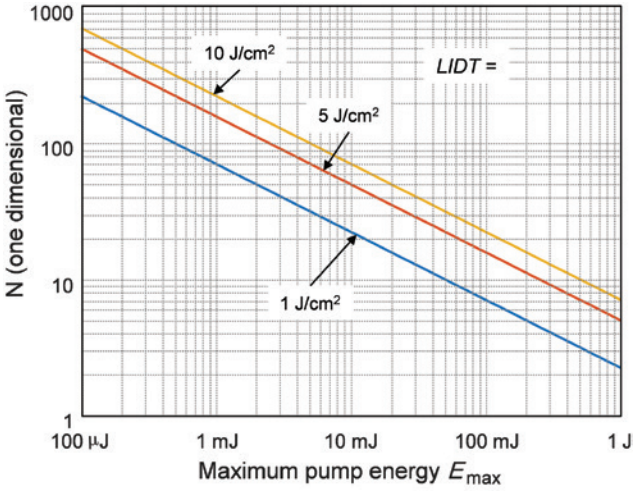

Figure 2: Number of resolved points (N) in 1D as a function of the maximum pump energy. The curves are plotted for a 1.5 cm OPO aperture and for different values of the laser-induced damage threshold (LIDT).

1 mJ range → 150 resolved points in each direction

10 mJ range → 45 resolved points in each direction

100 mJ range → 15 resolved points in each direction.

2.2.2 Choice of the nonlinear crystal

Most of the crystals used in OPOs are birefringent; this property being exploited to fulfill the phase-matching condition. The choice of the propagation direction in the crystal allows the choice of the operating signal and idler frequencies. Many materials are available for the visible (BBO, LBO, CLBO, COB, etc.), the near infrared ($LiNbO_3$, $KNbO_3$, $LiTaO_3$, KTP, KTA, RTA, CTA, etc.), and for the far infrared ($ZnGeP_2$, $AgGaSe_2$, $AgGaS_2$, GaSe, TAS, etc.). In addition, the technique of periodic poling has made possible the use of quasi-phase matching. First developed in $LiNbO_3$ (PPLN), it is now applied to KTP, $LiTaO_3$, KTA, RTA, GaAs, etc. The quasi-phase-matching technique allows exploiting the highest nonlinear coefficient of the material while avoiding walk-off issues [14]. Moreover, some recent publications show the successful growth of up to 10-mm-thick periodically poled (PP) crystals, leading to OPO optical-to-optical efficiency higher than 70% [15]. Commercially available materials developed for quasi-phase matching generally have an aperture, which has a limited size in one direction (typically from 500 µm to 1–3 mm). This would make PP materials appropriate candidates only for 1D beam-steering OPO systems, the number of resolved points is proportional to the nonlinear crystal aperture size, as shown in the previous section.

The concept of FT-OPO with 2D beam steering is, thus, more appropriate to larger crystals. For this purpose, $LiNbO_3$, KTP, and KTA are among the most commonly used crystals to generate a signal around 1.5 µm and an idler around 3.5 µm.

KTP and KTA crystals are preferred over $LiNbO_3$ because they can operate with noncritical phase-matching condition, so with negligible walk-off angle and a large angular acceptance of more than 100 mrad.cm, and a good nonlinear coefficient of 3 pm/V. Finally, for efficient operation around 3.5 µm, KTA is the best material candidate because of its good transparency window in this spectral range.

According to these requirements, an experimental setup has been realized using a 15 mm × 15 mm × 20 mm KTA crystal.

3 Experiments of beam steering with wavelength conversion in a FT-OPO

3.1 Experimental setup

The constructed OPO shown in Figure 3 is formed by an x-cut KTA crystal having an aperture of 15 mm × 15 mm and an interaction length of 20 mm from Cristal Laser (Messein, France). The crystal is inserted in a 40-mm-long linear cavity formed by two plane mirrors. The first (input) mirror of the cavity is anti-reflection (AR) coated at 1.06 µm and high reflection (HR) coated at 1.53 µm to ensure oscillation of the signal beam inside the cavity. The second (output) mirror is AR coated at 1.064 µm and 3.47 µm and partially reflective at 1.53 µm. Input and output mirrors are, respectively, made in fused silica and CaF_2 substrates to ensure a high transmission in the respective 1-µm and 3.47-µm spectral ranges. In the pump pulse duration time, the recirculating 1.53-µm signal pulse operates roughly five round trips in the cavity. The spatial overlap between pump and signal pulses in that time is ensured by gain guiding in the KTA.

The FT experimental setup is illustrated in Figure 4. The incident pump beam at 1.064 µm is delivered by a single-frequency Q-switched flash-lamp pumped Nd:YAG master-oscillator power amplifier (MOPA) laser system delivering 20-ns pulses at 50-Hz pulse repetition

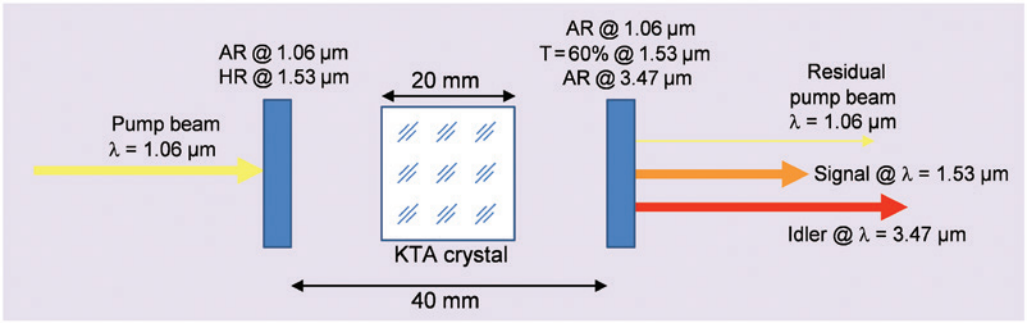

Figure 3: Schematic of the OPO formed by a KTA nonlinear crystal and by two plane mirrors.

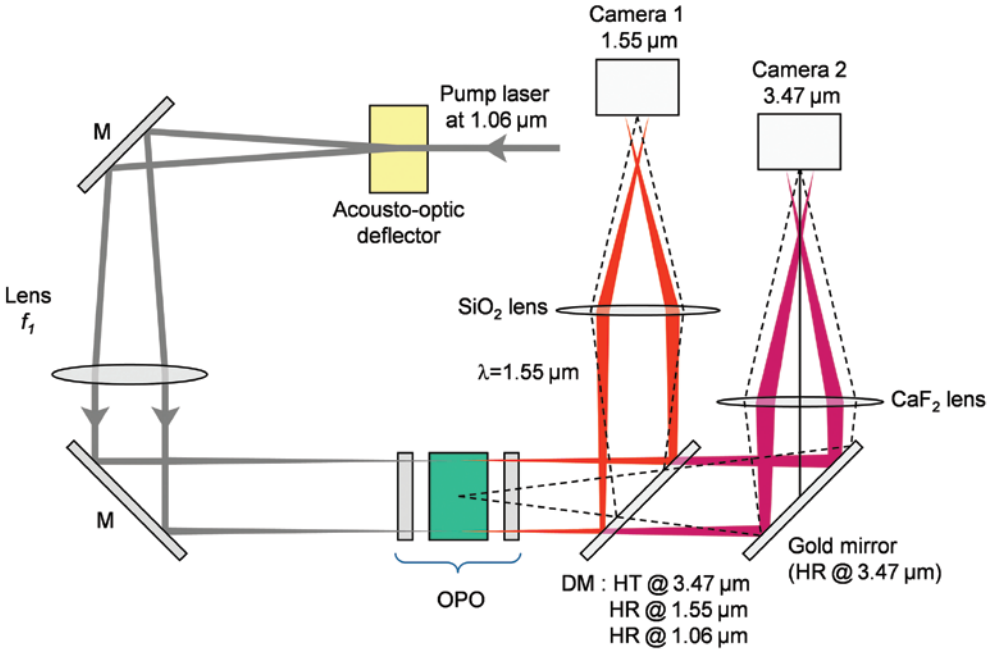

Figure 4: FT-OPO experimental setup with beam-steering capability at 1.53 µm and 3.47 µm. M, HR mirror at 1 µm; DM, dichroic mirror.

frequency (PRF). The 1-µm pump beam is deflected by means of an acousto-optic cell (TeO_2 2D AO scanner from AA Opto-electronic, model DTSX-400, with 50% diffraction efficiency over 49 mrad scan angle). The AO cell is placed in the object focal plane of a first lens with focal length $f_1 = 1$ m, while the middle plane of the OPO is placed in the Fourier plane of lens f_1.

The deflection of the 1-µm pump beam is converted into a displacement inside the OPO by lens f_1. The 1-µm pump spot size measurement in the KTA crystal gives a diameter of 525 µm. After wavelength conversion is performed inside the OPO, dichroic mirrors are used to separate the signal (1.53 µm) and idler (3.47 µm) and to cut the remaining pump. The displacement of the signal and idler beams are then back-converted into deflection by placing second lenses with focal length $f_2 = 25$ cm in a Fourier arrangement, to image the KTA crystal middle plane onto 1.55-µm and 3.47-µm cameras. These second lenses are, respectively, made of fused silica and CaF_2 for signal and idler paths. Alternatively, pyro-electric detectors are used for pulse-energy measurements.

3.2 Energetic performances of the OPO

The pulse energies at 1.53 µm and 3.47 µm are measured as a function of the pump pulse at 1.06 µm for a pump beam diameter of 525 µm in the KTA crystal. The experimental results are shown in Figure 5. The OPO threshold is 3.5 mJ incident pump pulse energy. At 6.65 mJ pump energy, a maximum of 1.94 mJ was obtained at 1.53 µm and 355 µJ at 3.47 µm. In this case, the fluence in the OPO crystal is

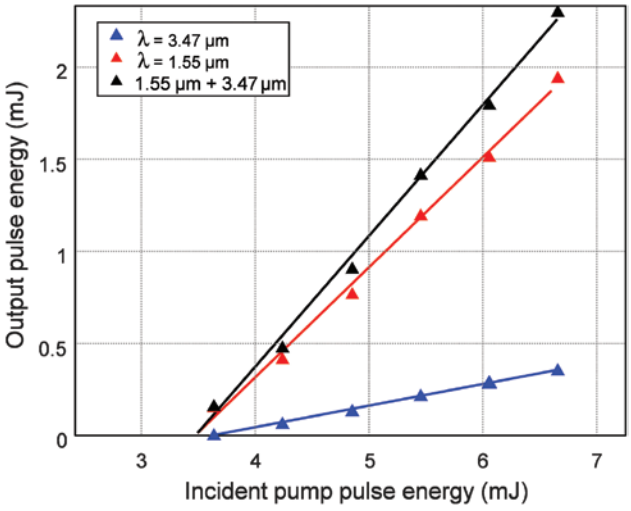

Figure 5: Signal + idler pulse energy as a function of the pump pulse energy. The pump beam diameter in the OPO is 525 µm.

3 J/cm^2. No LID was observed after several days of (non-continuous) operation.

These results indicate 29% and 5.3% conversion efficiencies, respectively, at 1.53 µm and 3.47 µm of the OPO itself. When the 50% diffraction efficiency of the AO cell is taken into account, the system overall beam-steering efficiencies from a nondeflected 1-µm pulse into a deflected pulse at 1.53 µm and 3.47 µm are 15% and 2.8%, respectively.

3.3 Beam steering at 1.53 µm and 3.47 µm

As the pump beam is deflected by the AO cell, the output converted and deflected signal and idler pulses are simultaneously monitored by, respectively, a phosphor-coated CCD and a pyroelectric camera. Figure 6 shows successive recorded images of the KTA crystal middle plane for one axis beam steering at 1.55 and 3.47 µm, with 6 mJ of incident pump pulse energy. Similar results are obtained for the other axis. The corresponding pulse energies vs. displacements (i.e. deflection) are plotted in Figure 7, both for the signal and for the idler. In both cases, it can be seen that over the entire size of the KTA crystal, the signal pulse energy is rather flat with mean values at 1.75 mJ ± 9% and 320 µJ ± 11%, respectively, for the signal (1.55 µm) and for the idler (3.47 µm).

The maximum beam-steering capability is given by the displacement excursion $\Delta = 15$ mm, which is clearly limited by the crystal size. Assuming a signal beam diameter equal to the pump beam diameter, the number of resolved directions N in each axis is given by:

$$N = \frac{\Delta}{2\omega_0} \times \sqrt{\frac{2}{\ln 2}}$$

With $2\omega_0 = 525$ µm, the number of resolved directions in each direction of the FT-OPO is 50 at the signal wavelength of 1.53 µm. When translated into angular capability using

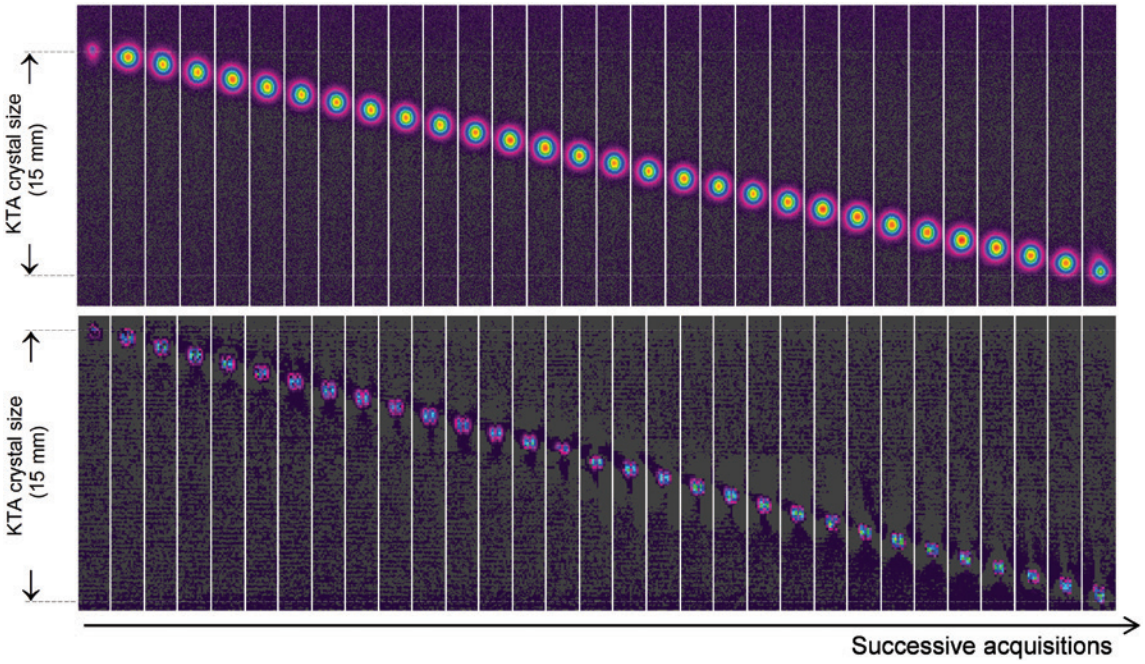

Figure 6: Beam deflection at 1.53 µm (top) and 3.47 µm (bottom) using the FT OPO for a 15 × 15 × 20 mm KTA crystal and a pump beam diameter of 525 µm. The vertical scale is given normalized to the size of the crystal.

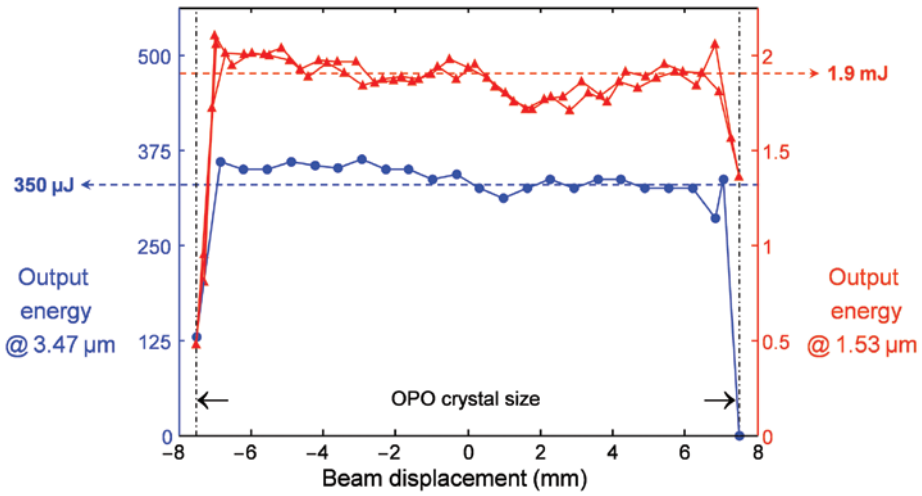

Figure 7: Beam-steering performances of the FT-OPO operating at 1.53 µm (left) and 3.47 µm (right) for a 15×15×20-mm KTA crystal and a pump beam diameter of 525 µm.

Figure 8: The 2D laser marking at 3.47 µm on a pyroelectric camera damage test plate.

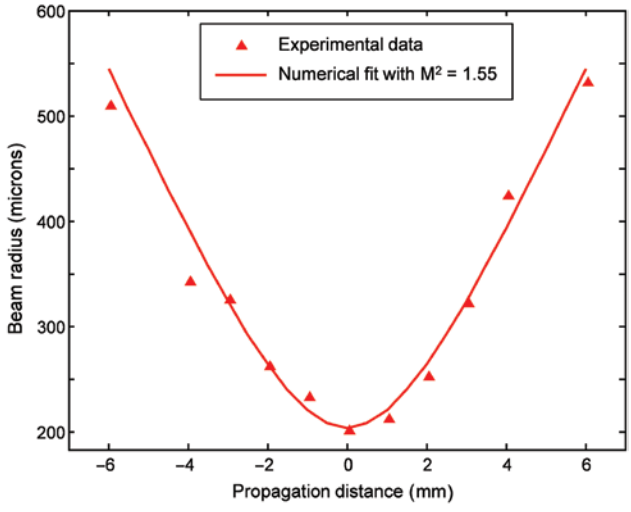

Figure 9: The 3.47-µm beam quality measurement.

the second lens L2 of focal length f_2, the angular scanning range θ is given by $\sin(\theta)=\Delta/(2f_2)$. This scanning range (of a bit less than $\pm 2°$ with $f_2=25$ cm in our case) can be tailored by an appropriate choice of lens.

At the idler wavelength of 3.47 µm, the spot size in the KTA crystal plane is measured using the knife edge method, leading to a beam radius ω_0 of 275 µm. According to the above equation, we obtain 46 resolved directions in each axis at 3.47 µm. In order to illustrate the 2D steering capability of the system, a pyroelectric camera damage plate is placed in the image plane of the KTA crystal, in the idler (3.47 µm) path. Figure 8 shows the plate after a 2D pattern is programmed on the AO cell drivers.

3.4 Beam quality of the deflected beam at 3.47 µm

Beam quality degradation of the converted beams can eventually appear in OPO systems due to thermal effects in the NL crystal. To evaluate this effect, the M^2 parameter of the 3.47-µm idler beam is determined by measuring the 3.47-µm beam size (using the knife edge method) as a function of the propagation distance. The resulting beam quality measurement is shown in Figure 9. A beam quality $M^2=1.55$ is obtained for the deflected 3.47-µm beam having 355 µJ pulse energy.

3.5 Demonstration of multitarget capability

The FT-OPO also offers the possibility of delivering several deflected beams for multitarget designation for

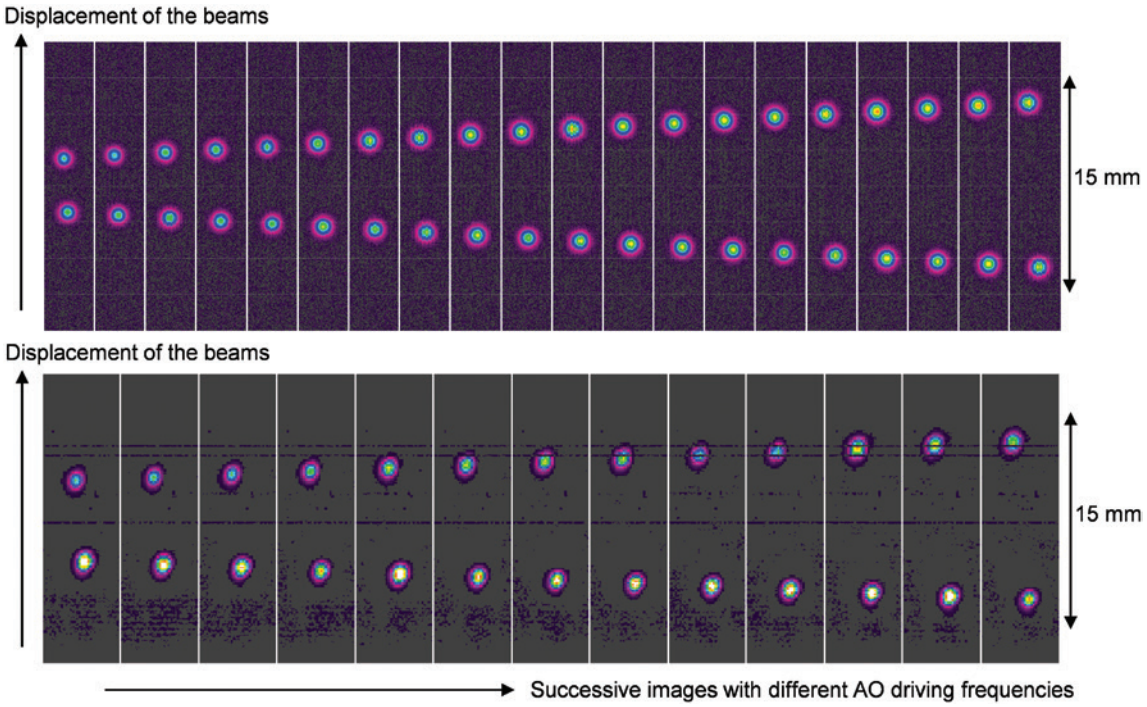

Figure 10: Illustration of the FT-OPO multibeam steering capability for the signal (top) and the idler (bottom).

instance. In order to demonstrate this property, two distinct driving frequencies were applied to the AO cell to generate two separate deflected beams at 1.06 µm. In order to maintain the same conversion efficiency in the OPO, the incident pulse energy on the AO cell was increased to 25 mJ. Under these conditions, the 1-µm pulse energy after diffraction onto the AO cell is 6 mJ in each of the deflected pump beams, so these are identical to previous single-pump beam experiments. The two deflected 1-µm beams were then sent to the OPO. Because of the action of lens 1, the two 1-µm beams were pumping the OPO at different positions, thus, generating two separate signal and idler beams. By changing the two driving frequencies, the multitarget beam deflection at 1.53 µm is recorded as shown in Figures 10 and 11. Note that the two directions are addressed simultaneously. As for the single-beam experiments, the energy in each of the two steered beams is 1.75 mJ for the signal and 320 µJ for the idler at 3.47 µm. Both are very stable over the entire deflection range.

4 Conclusion

A FT-OPO operating with a deflected 1-µm pump laser beam has been realized and fully characterized. This architecture allows converting the 1-µm laser beam into deflected beams around 1.5 µm and in the 3–5 spectral range. The power of this concept is to perform the nonmechanical deflection at a wavelength where efficient steering devices are available, like acousto-optic cells. The FT-OPO system then enables to reach spectral regions were direct nonmechanical steering means are still problematic, like the mid-IR in this work. It is worthwhile mentioning that the present concept would also apply for all kinds of nonlinear interactions, such as frequency doubling or tripling and could generate a UV scanner.

By using a large KTA crystal with 15 mm × 15 mm aperture, beam steering has been demonstrated at 1.53 µm and 3.47 µm. The number of resolved direction per axis is about 50 for both wavelengths, i.e., a total of 2500 resolved points, limited by the nonlinear crystal size. The FT-OPO proved very flat pulse energies over the full deflection range, with nearly 2 mJ and 350 µJ at 1.53 µm and 3.47 µm, respectively, for an input pump pulse energy of about 7 mJ at 1 µm. Moreover, we showed that the system does not introduce significant beam quality degradation, with an idler M^2 of 1.55 measured at 3.47 µm. As nonlinear interaction can be considered instantaneous, random access time to any IR beam direction is dictated by the primary pump steering device, 10 µs with our AO cell. Finally, as the FT architecture by essence converts an angular

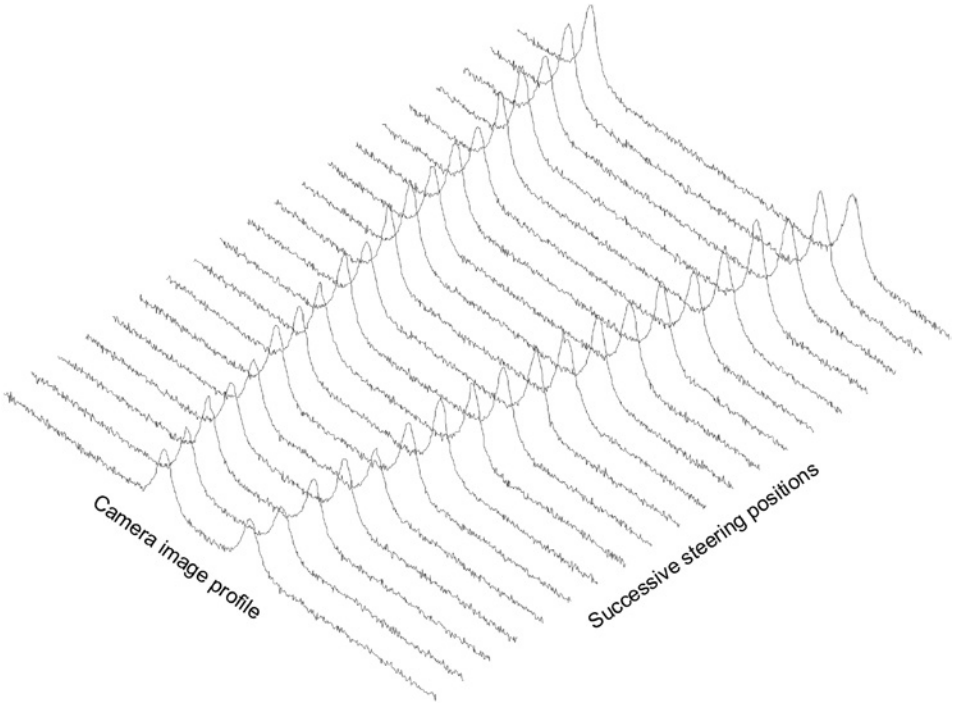

Figure 11: Intensity profiles of the successive images of Figure 10 for the signal case (1.53 μm).

variation of a beam into a displacement in the NL crystal, multiple beams with different angles never overlap in the crystal, which enables the demonstrated property of efficient simultaneous multiple beam steering of the system.

This laser setup demonstrates fast μs nonmechanical beam steering in mid-IR with attractive characteristics required in diversity applications such as laser remote sensing, multitarget designation, or material processing.

Acknowledgments: The authors acknowledge the French, Italian, and German MODs for financial support of this work through the ATLAS EDA/EUROPA MOU – RTP 108.085 project.

References

[1] H. D. Tholl, Proc. SPIE 6397, 1–14 (2006).
[2] M. Gottlieb, C. Ireland and J. Ley, 'Electro-Optic and Acousto-Optic Scanning and Deflection', (Marcel Dekker Publishing, New York, 1983).
[3] P. Maák, L. Jakab, P. I. Richter, A. Brignon and J.-P. Huignard, Opt. Commun. 176, 163–169 (2000).
[4] F. Chen, J. Geusic, S. Kurtz, J. Skinner and S. Wemple, J. Appl. Phys. 37, 388–398 (1996).
[5] Y. Ninomiya, *IEEE* J. Quantum Elec. 9, 791–795 (1973).
[6] D. Djukic, R. Roth, J. Yardley, O. J. Roberts, S. Bakhru, et al., Opt. Express 12, 6159–6164 (2004).
[7] S. R. Davis, G. Farca, S. D. Rommel, S. Johnson and M. H. Anderson, Proc. SPIE 7618, 1–14 (2010).
[8] D. P. Resler, D. S. Hobbs, R. C. Sharp, L. J. Friedman and T. A. Dorschner, Opt. Lett. 21, 689–691 (1996).
[9] J. Bourderionnet, M. Rungenhagen, D. Dolfi and H. D. Tholl, Proc. SPIE 7113, 1–11 (2008).
[10] J. A. Thomas, M. E. Lasher, Y. Fainman and P. Soltan, Proc. SPIE 3131, 124–132 (1997).
[11] R. Byer, in 'Quantum Electronics: A Treatise', vol. 1, (Academic Press, New York, 1975) pp. 588–694.
[12] J. Raffy, T. Debuisschert and J.-P. Pocholle, Opt. Let. 22, 1589–1591 (1997).
[13] A. Brignon and J.-P. Huignard, 'Laser beam deflecting with frequency conversion' Patent EP1425628B1, 2002.
[14] A. Zukauskas, N. Thilmann, V. Pasiskevicius, F. Laurell and C. Canalias, in 'Advanced Solid-State Photonics, paper JWB1', (Istanbul, 2011).
[15] H. Ishizuki and T. Taira, Opt. Express 20, 20002–20010 (2012).